Biochimie 94 (2012) 155–165

Contents lists available at SciVerse ScienceDirect

Biochimie

journal homepage: www.elsevier.com/locate/biochi

Research paper

Crystal structure and molecular dynamics studies of purine nucleoside phosphorylase from *Mycobacterium tuberculosis* associated with acyclovir

Rafael A. Caceres [a,b], Luís F.S.M. Timmers [a,c], Rodrigo G. Ducati [d], Diego O.N. da Silva [e], Luiz A. Basso [b,c,d], Walter F. de Azevedo Jr. [a,b,c,*], Diógenes S. Santos [b,c,d,*]

[a] *Faculdade de Biociências, Laboratório de Bioquímica Estrutural, Pontifícia Universidade Católica do Rio Grande do Sul, Porto Alegre - RS, Brazil - Instituto Nacional de Ciência e Tecnologia em Tuberculose (INCT-TB), Brazil*
[b] *Programa de Pós-Graduação em Medicina e Ciências da Saúde, Pontifícia Universidade Católica do Rio Grande do Sul, Porto Alegre - RS, Brazil*
[c] *Programa de Pós-Graduação em Biologia Celular e Molecular, Pontifícia Universidade Católica do Rio Grande do Sul, Porto Alegre - RS, Brazil*
[d] *Centro de Pesquisas em Biologia Molecular e Funcional (CPBMF), Instituto de Pesquisas Biomédicas, Pontifícia Universidade Católica do Rio Grande do Sul, Porto Alegre - RS, Brazil – Instituto Nacional de Ciência e Tecnologia em Tuberculose (INCT-TB), Brazil*
[e] *Universidade Católica de Brasília, Brasília - DF, Brazil*

ARTICLE INFO

Article history:
Received 3 June 2011
Accepted 11 October 2011
Available online 20 October 2011

Keywords:
Purine nucleoside phophorylase
Mycobacterium tuberculosis
Crystallographic structure
Acyclovir
Molecular dynamics

ABSTRACT

Consumption has been a scourge of mankind since ancient times. This illness has charged a high price to human lives. Many efforts have been made to defeat *Mycobacterium tuberculosis* (Mt). The *M. tuberculosis* purine nucleoside phosphorylase (MtPNP) is considered an interesting target to pursuit new potential inhibitors, inasmuch it belongs to the purine salvage pathway and its activity might be involved in the mycobacterial latency process. Here we present the MtPNP crystallographic structure associated with acyclovir and phosphate (MtPNP:ACY:PO_4) at 2.10 Å resolution. Molecular dynamics simulations were carried out in order to dissect MtPNP:ACY:PO_4 structural features, and the influence of the ligand in the binding pocket stability. Our results revealed that the ligand leads to active site lost of stability, in agreement with experimental results, which demonstrate a considerable inhibitory activity against MtPNP (K_i = 150 nM). Furthermore, we observed that some residues which are important in the proper ligand's anchor into the human homologous enzyme do not present the same importance to MtPNP. Therewithal, these findings contribute to the search of new specific inhibitors for MtPNP, since peculiarities between the mycobacterial and human enzyme binding sites have been identified, making a structural-based drug design feasible.

1. Introduction

Tuberculosis (TB) resurged in the late 1980s, and the World Health Organization has declared it as a global emergency. TB causes 9.4 million new infections and kills almost two million people a year, standing behind, among infectious diseases, only to AIDS [1]. It is estimated that one-third of the world's population (approximately two billion individuals) is infected with *Mycobacterium tuberculosis* (Mt). About 5–10% of the infected individuals develop active TB during lifetime, as a result of latent infection reactivation. However, the risk of developing the disease to those co-infected with the human immunodeficiency virus (HIV) increases to 5–15% annually. The high susceptibility of HIV infected people to TB and the proliferation of multidrug-resistant strains have created a worldwide interest in expanding current TB research programs. New antimycobaterial agents are needed to confront *M. tuberculosis* strains resistant to existing drugs and to shorten the treatment course in order to improve patient's compliance [2,3].

Homologue enzymes in the purine salvage pathway have been identified in the *M. tuberculosis* genome sequence [4]. Purine nucleoside phosphorylase (PNP), a component enzyme of this pathway, was identified to play a central role in purine metabolism. The salvage pathway represents an essential cellular process that is crucial for many organisms, and its proteins could be implicated in mycobacterial latency [5]. Thereby, PNP might represent an attractive molecular target and offer an opportunity to overcome this illness. In *M. tuberculosis*, this enzyme (MtPNP) is responsible for catalyzing the reversible phosphorolysis of *N*-glycosidic bonds of purine (deoxy)ribonucleosides, except adenosine, in the presence of inorganic phosphate (PO_4), to generate (deoxy)ribose 1-phosphate and the corresponding purine base [6–10]. It is

* Corresponding authors. Av. Ipiranga 6681, CEP 90619-900, Porto Alegre – RS, Brazil. Tel./fax: +55 51 3320 3629.
E-mail addresses: walter@azevedolab.net (W.F. de Azevedo Jr.), diogenes@pucrs.br (D.S. Santos).

0300-9084
doi:10.1016/j.biochi.2011.10.003

specific for purine nucleosides in the β-configuration and cleaves the glycosidic bond with inversion of configuration to produce α-(deoxy)ribose 1-phosphate [11].

Potent inhibitors of PNP from different sources are frequently structural analogues of nucleoside substrates, base and/or pentose moiety modifications. Nevertheless the development of new potent selective inhibitors for MtPNP is still a scientific endeavor as they may present high toxicity, thereby becoming inappropriate for human administration. Accordingly, efforts to develop drugs with selective toxicity based on structural differences between MtPNP and the human homologue (HsPNP) should be pursued. A number of research groups have dedicated their efforts to determine specificity of substrates, kinetic mechanisms, and three-dimensional structures for PNPs from different bacterial sources [12–20] in comparison to HsPNP. Even though PNP activity is shared between humans and *M. tuberculosis*, drugs with selective toxicity against the mycobacterial enzyme can still be developed if one takes advantage of singular features that make them dissimilar [21].

The 9-(2-hydroxy-ethoxy-methyl)guanine, also known as acyclovir (ACY) (Fig. 1), is a synthetic nucleoside analogue with a 9-substituent acyclic chain, and is an useful clinical antiherpetic agent that has been employed as a HsPNP inhibitor with moderate activity in erythrocytes ($K_i = 91$ μM) [22].

In accordance with this statement, this work describes the crystallographic structure of MtPNP associated with ACY, which can be a possible MtPNP inhibitor. Molecular dynamics (MD) simulation was also performed in order to provide an insight into its complex behavior under solution, giving valuable information around the MtPNP atomic features. The principal component analysis (PCA) was assessed through MD, aiming to extract the preponderant movements and, consequently, analyze the conformational changes when comparing the structure in the free form and complexed with ACY. Furthermore, all these analysis can support bases for a greater knowledge concerning this enzyme, providing new insights into its active site, and might guide future efforts to design selective and potential inhibitors for the mycobacterial enzyme, based on the structure of ACY.

2. Materials and methods

2.1. Crystallization and data collection

MtPNP:ACY:PO_4 was crystallized using the experimental conditions described elsewhere [13,19]. PNP solution was concentrated to 25 mg/mL and co-crystallized with ACY. Hanging drops were prepared by mixing 1 μL of protein solution and 1 μL of reservoir solution (100 mM Tris pH 8.0 25% PEG3350 25 mM $MgCl_2$). The crystal was flash frozen at 100 K. X-ray diffraction data were collected at 1.427 Å wavelength using Synchrotron Radiation Source (Laboratório Nacional de Luz Síncrotron, Campinas – SP, Brazil) and a CCD detector (MARCCD). The crystal diffracted at 2.10 Å and the data were processed using Mosflm, and scaled with the Scala [23] programs.

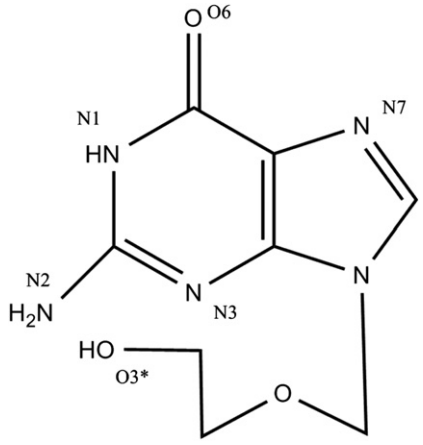

Fig. 1. Molecular formula of acyclovir.

2.2. Structure resolution and refinement

The crystal structure of MtPNP:ACY:PO_4 was determined by standard molecular replacement using the AMoRe software [24] and the structure of MtPNP complexed with 9-deazahypoxanthine (PDB code: 1I80 [19]) as a template. Structure refinement was performed using the Refmac5 software [23]. The atomic positions obtained from molecular replacement were used to initiate the crystallographic refinement. The overall stereochemical quality of the final model was assessed by the Procheck software [25].

2.3. Molecular dynamics simulation protocol

MD simulations were performed with the MtPNP trimeric structure to provide a more realistic analysis, since this enzyme is biologically active as a trimer [13,19]. Two systems were built, the first composed by MtPNP apoenzyme (the PO_4 ions and ACY were removed from the crystallographic structure), and the second by MtPNP, PO_4 ion, and ACY (MtPNP:ACY:PO_4). The homotrimeric structures provide a remarkable analysis possibility, since the systematic association of each ligand on each monomer leads to specific conformational changes in the same structure. Based on this, in monomer B, the PO_4 ion, and in monomer C, the PO_4 ion and ACY, were retrieved, allowing the evaluation of the influence of ACY and PO_4 to the conformational changes. The MD simulations were carried out in periodic boundary conditions using Gromacs 4.0.5 [26,27] package with Gromos 96.1 (53A6) force field [28]. The molecular topology file and force field parameters were generated by the Prodrg program [29] except the ACY charges. The ACY partial atomic charges were determined by using the ChelpG method [30], implemented in the Gaussian W03 program [31], at DFT/B3LYP/6-31G** level. Before the MD simulations, the structures were solvated with the explicit SPC/E water model [32] embedded in 79.56 Å × 73.82 Å × 52.14 Å cubic box, in which the minimum distance between the protein surface and the box face was 10 Å in both cases. The simulation systems were composed of 31,121 (MtPNP) and 31,102 (MtPNP:ACY:PO_4) water molecules. In both systems, Na^+ counter ions were added using Genion program of the Gromacs simulation suite to neutralize the negative charge density of these systems.

The systems were then submitted to a steepest descent followed by conjugated gradient energy minimization down to a tolerance of 1000 kJ/mol, step by step. The entire systems were minimized to remove close van der Waals contacts followed by a short MD simulation with position restrains for a period of 20 ps. Each system was heated with gradual increments in the following temperatures: 100 K (10 ps), 150 K (10 ps), 200 K (10 ps), 250 K (10 ps), and 300 K (10 ps). Thereafter, the temperatures of the systems were adjusted to 310 K, and the velocities at each step were reassigned according to the Maxwell–Boltzmann distribution. The temperatures of solvent and solutes (MtPNP, ACY, and PO_4) were independently coupled to a thermal bath with a relaxation time of 0.1 ps using a velocity rescale thermostat [33]. The pressure in the systems was weakly coupled to a pressure bath of 1 atm by applying an isotropic scaling and 0.5 ps relaxation time using the Berendsen barostat [34].

Afterwards, full MDs without restrains were carried out. These were performed under normal temperature (310 K) and pressure (1 bar) using a temperature coupling time constant of 0.1 ps and

a pressure coupling time constant of 1.0 ps. The value of the isothermal compressibility was set to 4.5×10^{-5} bar^{-1} for water simulations. All bond lengths, including hydrogen atoms, were constrained by the LINCS algorithm [35]. The electrostatic interactions were calculated by using the Particle mesh Ewald algorithm [36], with interpolation order of 4 and a grid spacing of 1.2 Å. The cutoff for van der Waals interactions was 14 Å. All simulations were performed for 20 ns with a time step of 2 fs, and coordinates were saved every 0.5 ps. All systems were simulated in NPT ensemble.

All analyses were performed on the ensemble of system configurations extracted at 0.5 ps time intervals from the simulation. The convergence of both simulations was analyzed in terms of the secondary structure, root mean-square deviation (RMSD) from the initial model structures, and radius of gyration (RG). The MD simulation and analyses were performed in a DuoQuad Core 550 Xeon–3.00 GHz server. Examinations and repairs of the molecular structures were achieved using the Swiss PDBViewer v4.0 [37], VMD [38], and PyMOL [39] programs. Analyses were performed using the features within the GROMACS package.

2.4. Principal component analysis

Protein functions are embedded in their structure and a major goal of protein simulation is to generate enough configurations of the system of interest to extract functionally relevant motions. One such tool for reducing the generated dimensionality of MD trajectory to an essential subspace encompassing few degrees of freedom, eliminating the positional fluctuations, is PCA [40], which is a method commonly used for dissecting the dynamics of proteins and their importance in biological processes, like protein folding or substrate binding. The PCA analysis is a technique that reduces the complexity of the data and extracts the concerted motion in simulations that are essentially correlated and presumably meaningful for biological function [41]. In the PCA analysis, a variance/covariance matrix was constructed from the trajectories after removal of the rotational and translational movements. A set of eigenvectors and eigenvalues was identified by diagonalizing the matrix. The eigenvalues represented the amplitude of the eigenvectors along the multidimensional space, and the displacements of atoms along each eigenvector showed the concerted motions of protein along each direction. An assumption of PCA analysis is that the correlated motions for the function of the protein are described by eigenvectors with large eigenvalues. The protein movements in the essential subspace were identified by projecting the Cartesian trajectory coordinates along the most important eigenvectors from the analysis. PCA was performed using analysis tools from the GROMACS package, considering only the backbone atoms for generating the covariance matrix. Prior to performing PCA, all translations and rotational motions were eliminated by fitting the trajectory to a reference structure, in this case, the average structure.

2.5. Experimental materials

All chemicals were of analytical or reagent grade and were used without further purification. Inosine and ACY were acquired from Sigma. Recombinant MtPNP was expressed and purified as previously described [14]. The steady-state activity assays were carried out in a UV-2550 UV–visible Spectrophotometer and the fluorescence binding assays were carried out in an RF-5301PC Spectrophotometer, both from Shimadzu.

2.6. Enzyme activity assays

All enzyme activity assays were carried out under initial rate conditions at 25 °C in 100 mM Hepes pH 7.0 (500 μL total reaction volumes), and each individual datum is the average of duplicate or triplicate measurements. The phosphorolysis of Inosine to Hypoxanthine ($\varepsilon = 1000$ M^{-1} cm^{-1} at 280 nm), in the presence of PO_4 and MtPNP, was monitored spectrophotometrically by a time-dependent decrease in absorbance [14]. In order to evaluate its inhibitory effect, the concentration of ACY that reduces enzyme activity by half (IC_{50}) was determined by measuring initial velocity rates at Inosine (40 μM) and PO_4 (600 μM) concentrations close to their K_M values [14] in either absence or presence of ACY (12–40 μM). The inhibition pattern was determined by measuring initial velocity rates at varying Inosine concentrations (20–600 μM), a fixed non-saturating PO_4 concentration (600 μM), and fixed-varying inhibitor concentrations (0–48 μM). For both inhibition experiments, reactions were initiated by the addition of MtPNP (55 nM) into the reaction mixture.

2.7. Fluorescence spectroscopy

Fluorescence titration of MtPNP by ACY was carried out at 25 °C by making microliter additions of 0.5 mM and 2.0 mM ACY stock solutions (final concentration ranging from 0.25 to 178.41 μM) to 2 mL of 3 μM MtPNP in 100 mM Hepes pH 7.0, keeping the dilution to a maximum of 10.0%. Measurements of intrinsic protein fluorescence of MtPNP employed excitation wavelength at 290 nm and emission wavelength ranging from 320 to 400 nm (maximum $\lambda_{EM} = 334$ nm). The slits for excitation and emission wavelengths were, respectively, 15 and 1.5 nm. To account for the inner filter effect due to ACY absorption of excitation light, two cuvettes were placed in series so that the contents of the first cuvette (either buffer or ACY) acted as a filter of the excitation light and the light from the second cuvette detected.

2.8. Experimental data analysis

The kinetic parameter values and their respective standard errors were obtained by fitting the data to the appropriate equations by using the nonlinear regression function of SigmaPlot 2004 (SPSS, Inc.). Data obtained in the inhibition pattern studies were properly fitted to Eq. (1), which describes a competitive inhibition, where v is the measured reaction velocity, V is the maximal velocity, A is the substrate concentration (either Inosine or PO_4), K_a is the substrate's Michaelis constant, I is the inhibitor concentration, and K_{is} is the slope inhibition constant.

$$v = VA/[K_a(1 + I/K_{is}) + A] \quad (1)$$

Data from equilibrium fluorescence spectroscopy were fitted to Eq. (2), the Hill equation [41], in which F is the observed fluorescence signal, F_{max} is the maximal fluorescence, F/F_{max} ratio is the degree of saturation, n represents the total number of binding sites, and K' is the mean dissociation constant for MtPNP:ACY binary complex formation, which is comprised of interaction factors and the intrinsic dissociation constant.

$$F/F_{max} = A^n/(K' + A^n) \quad (2)$$

3. Results and discussion

3.1. Molecular replacement and crystallographic refinement

The MtPNP:ACY:PO_4 structure was solved by molecular replacement with the AMoRe software [24] using the crystallographic structure of MtPNP complexed with 9-deazahypoxanthine (PDB code: 1I80 [19]) as a template. The crystal diffracted at 2.10 Å

resolution and belongs to orthorhombic space group P 2_12_12. Model building was performed with the MIFiT 3.1.0 program [42] using $F_{obs} - F_{calc}$ and $2F_{obs} - F_{calc}$ density maps that show the electron density for ACY and PO_4 in the structure (Fig. 2B). Atomic coordinates for ACY and PO_4 ions have been included in the model and all crystallographic refinement using Refmac5 [23] continued with maximum likelihood protocol, followed by alternate cycles of positional refinement and manual rebuilding using MIFit 3.1.0 [42]. A total of 388 water molecules were added to the model. The final model had R_{free} and R_{factor} of 26.20% and 18.30%, respectively, and a correlation coefficient of 94.6%. The highest magnitude of the correlation coefficient function obtained for the Euler angles were $\alpha = 79.81°$, $\beta = 10.83°$, and $\gamma = 183.84°$. The fractional coordinates are $T_x = 0.0821$, $T_y = 0.3041$, and $T_z = 0.4043$.

Data collection and structure refinement are summarized in Table 1. The Matthews coefficient (V_m) is 1.63 Å^3 Da^{-1} assuming a trimer for the asymmetric unit and 24.55% of solvent content. Analysis of Ramachandran diagram φ–ψ for the structure indicates that 89.10% of the residues are in the most favored regions, 9.50% in the additional allowed regions, 0.80% in the generously allowed regions, and 0.60% in the disallowed regions of the plot. Analysis of the electron density map ($2F_{obs} - F_{calc}$) agrees with the Thr209 of the three monomers, positioning this same residue in the disallowed regions in the other MtPNP structure previous solved [43].

3.2. Crystallographic structure of MtPNP:ACY:PO_4

The MtPNP:ACY:PO_4 structure follows the same fold as other MtPNPs described elsewhere [13,19,20,43]. The active sites of all known trimeric PNPs are located near the subunit interfaces, and there is one active site for each monomer near the subunit interfaces.

The data obtained from crystallography revealed that the structure is a trimer in the asymmetric unit (Fig. 3), like in solution [13,19], and each monomer displays an α/β fold consisting of

Table 1
Data collection and refinement statistics. Values in parentheses refer to the highest resolution shell.

X-ray wavelenght (Å)	1.427
Temperature (K)	100
Resolution range (Å)	33.94–2.10 (2.15–2.10)
Number of measurements with $>2\sigma$ (I)	288832
Number of independent reflections	31716
Space group	$P2_12_12$
Matthews coefficient (Å^3 Da^{-1})	1.63
Unit-cell parameters	
a (Å)	105.177
b (Å)	135.759
c (Å)	41.434
$\alpha = \beta = \gamma$ (°)	90
Highest Resolution Shell (Å)	2.10
Data completeness (%)	93.92
R_{sym} (%)[a]	5.80
R_{factor} (%)[b]	18.30
R_{free} (%)[c]	26.20
Number of ligands	3
Number of phosphate groups	3
Number of water molecules	435
Observed RMSD from the ideal geometry	
Bond lenghts (Å)	0.02
Bond angles (°)	2.39
B-factor values (Å)^2 [d]	
Average B value for main chain	22.47
Average B values for side chain	23.36
Average B values for acyclovir	34.30
Average B values for phosphate groups	47.35
Average B values for waters	25.54
Ramachandran Plot	
Residues in most favored regions (%)	89.10
Residues in additionally allowed regions (%)	9.50
Residues in generously allowed regions (%)	0.80
Residues in disallowed regions (%)	0.60

[a] $R_{sym} = 100\sum|I(h)-<I(h)>|/\sum I(h)$ with I(h), observed intensity and {$I(h)$}, mean intensity of reflection h overall measurement of $I(h)$.
[b] $R_{factor} = 100 \times \sum|F_{obs} - F_{calc}|/\sum(F_{obs})$, the sums being taken overall reflections with $F/\sigma(F) > 2$ cutoff.
[c] $R_{free} = R_{factor}$ for 10% of the data, which were not included during crystallographic refinement.
[d] B values = average B values for all non-hydrogen atoms.

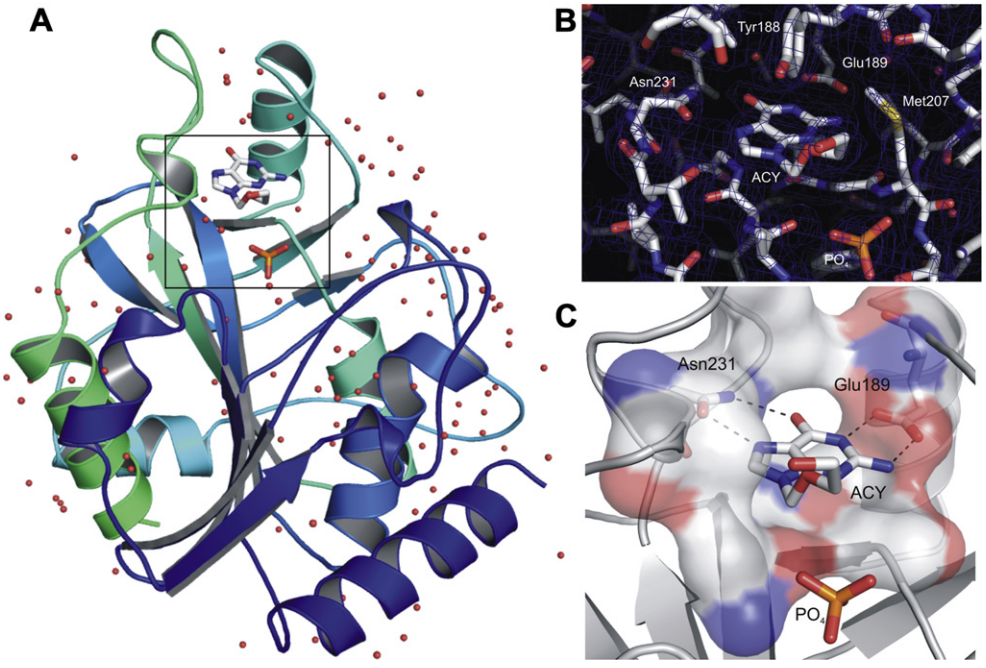

Fig. 2. (A) MtPNP monomer presented as cartoon; (B) MtPNP:ACY:PO_4 $2F_{obs} - F_{calc}$ electron density map contoured at 1σ; and (C) Classical MtPNP binding site presented as cartoon, and the residues Glu189, Asn231, and ACY as sticks.

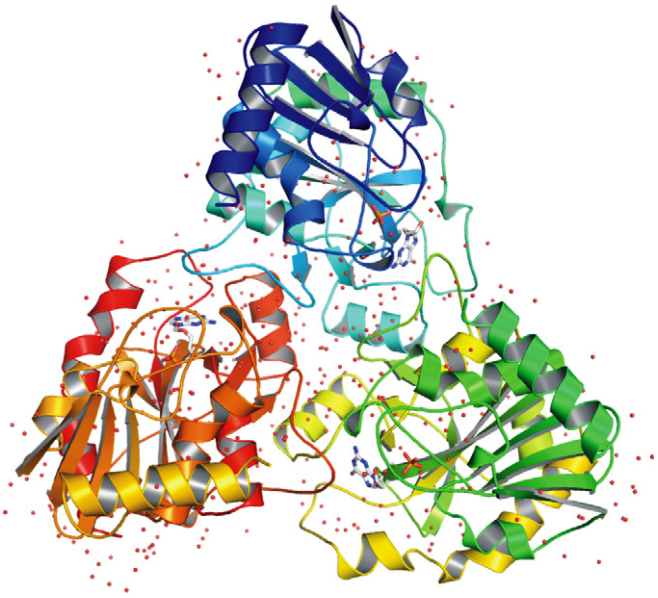

Fig. 3. Homotrimeric MtPNP:ACY:PO_4 schematic drawing. The MtPNP is presented as cartoon, and the ACY and PO_4 as sticks.

a mixed β-sheet surrounded by α-helices (Fig. 2A). The analysis of the electron density maps at final stages of the crystallographic refinement shows that the ligand (ACY) is positioned into the MtPNP classical binding site (Fig. 2C) anchored by the two binding pocket main residues (Glu189 and Asn231). Each active site contains one PO_4 and one ACY molecule.

3.3. Interactions of MtPNP with ACY and PO_4

The interactions between ACY and MtPNP were evaluated with the Ligplot program [44], which revealed four intermolecular hydrogen bonds between the ligand and the residues Glu189 and Asn231, and hydrophobic contacts with other residues of the binding pocket. All interactions are shown in Table 2. In addition, we observed that PO_4 binds beneath the inhibitor, in the active site, to stabilize the oxocarbenium transition-state and orients the nucleoside substrate [19]. Exceptionally in monomer A (Table 2), the MtPNP residues involved in hydrogen bonds with PO_4 are provided from loop regions, excluding Ala120. Analysis of hydrogen bonds showed that Arg88 and Ser208 interact with O1, while Ala120 interacts with O4 (monomer B) and O1 (monomer C). Although described in a previous work (MtPNP structure with Immucillin [19]), there seems to be no interactions between PO_4 and residues His90 and Ser36 in MtPNP:ACY.

The PO_4 substrate interactions from MtPNP crystallopgraphic structure were analyzed, and the PO_4 hydrogen bond interactions are shown in Table 2. As previously mentioned, the interactions between PO_4 and MtPNP do not follow the same pattern of interactions in the monomers.

We also evaluated the effect of the PO_4 substrate on drug-inhibitor binding of ACY to MtPNP. However, it should be pointed that, in the MtPNP:ACY:PO_4 system, the total interaction energy between the enzyme and the inhibitor was calculated in the presence of PO_4 in monomer A, and absence in the monomer B. As shown in Fig. 4, the association of a single PO_4 ion causes an increase of approximately 50 kJ/mol until 5 ns of MD simulation. A decrease of interaction energy occurs, suggesting that ACY is moving away from the active binding site.

Table 2
Hydrogen bonds and hydrophobic contacts of MtPNP:ACY:PO_4 monomers during MD simulations.

MtPNP→ACY				MtPNP→PO_4		
Hydrogen bond			Hydrophob. contact	Hydrogen bond		
Res (Chain)	Atom	Dist (Å)	Res (Chain)	Res (Chain)	Atom	Dist (Å)
Monomer A						
Glu189 (A)	OE1→N1	2.5	Ala120 (A)	Ala120 (A)	N→O2	3.1
	OE2→N2	2.5	Ala121 (A)			
			Gly122 (A)	Tyr180 (A)	OH→O4	3.4
Asn231 (A)	ND2→N7	3.1	Phe153 (B)			
	ND2→O6	3.0	Tyr188 (A)	Met207 (A)	N→O4	3.4
			Val205 (A)			
			Gly206 (A)	Ser208 (A)	OG→O1	2.8
			Met207 (A)			
			Leu241 (A)			
			Val246 (A)			
Monomer B						
Glu189 (B)	OE1→N1	2.4	Ser36 (B)	Ser36(B)	OG→O3	2.4
	OE2→N2	2.5	Ala120 (B)			
			Ala121 (B)	Arg88 (B)	NH1→O1	2.6
Asn231	OD1→N7	2.7	Phe153 (C)			
			Tyr188 (B)	Hi90 (B)	NE2→O1	3.4
			Val205 (B)			
			Gly206 (B)	Ala120 (B)	N→O4	2.6
			Met207 (B)			
				Ser208 (B)	OG→O3	2.6
Monomer C						
Glu189 (C)	OE2→N2	2.6	Ala120 (C)	Ser36(C)	OG→O4	2.8
			Ala121 (C)			
Asn231 (C)	OD1→N7	2.2	Gly122 (C)	Arg88 (C)	NH1→O4	3.0
	ND2→O6	2.6	Tyr188 (C)			
			Gly206 (C)	His90 (C)	NE2→O4	3.0
Thr230 (C)	OG1→N7	2.6	Met207 (C)			
			Val246 (C)	Ala120 (C)	N→O1	2.8
				Ser208 (C)	OG→O2	2.5

Distance cutoffs used for hydrogen bonding and hydrophobic interactions were 2.7–3.5 Å and 2.9–3.9 Å, respectively.

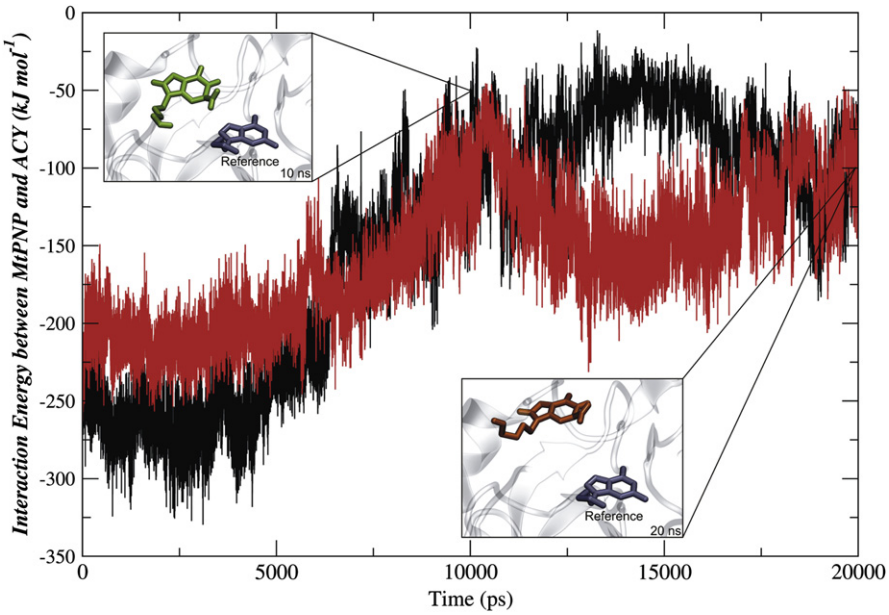

Fig. 4. Interaction energy between MtPNP and ACY. The black line represents the interaction energy between MtPNP and ACY of monomer A, and the gray line represents the interaction energy between MtPNP and ACY of monomer B (in absence of PO_4). The squares present the displacement of ACY away from the active site at 10 ns (green structure) MD simulation (top left) and at 20 ns (orange structure) MD simulation (bottom right) on monomer A, where the reference is ACY crystallographic structure. (For interpretation of the references to colour in this figure legend, the reader is referred to the web version of this article.)

3.4. Differences between HsPNP and MtPNP in complex with ACY

In order to evaluate the possible differences in the PNP structure from *Homo sapiens* and *M. tuberculosis*, the crystallographic structures were superposed (Fig. 5). The MtPNP:ACY:PO_4 was used as reference against HsPNP:ACY (PDB: 1PWY [45]). The water and PO_4 were omitted and the RMSD average for Cα superposition was 1.31 Å, at the purine binding site the RMSD average for Cα was 0.51 Å (MtPNP: Ala120, Ala121, Gly122, Glu189, and Asn231; and HsPNP: Ala116, Ala117, Gly118, Glu201, and Asn243). The major differences in the secondary structures of MtPNP and HsPNP are probably due to differences between the length of polypeptide chains, where HsPNP presents 21 amino acids more than MtPNP.

3.5. Molecular dynamics simulations

The MD simulations of free MtPNP and MtPNP:ACY:PO_4 ternary complex structures were performed using SPC/E water model, as previously described in section 2.3, and applying periodic boundary conditions.

The stability of the previous simulations was examined by conventional structural and geometrical analysis. Fig. 6 shows the RMSD of the Cα atomic positions for the MtPNP and

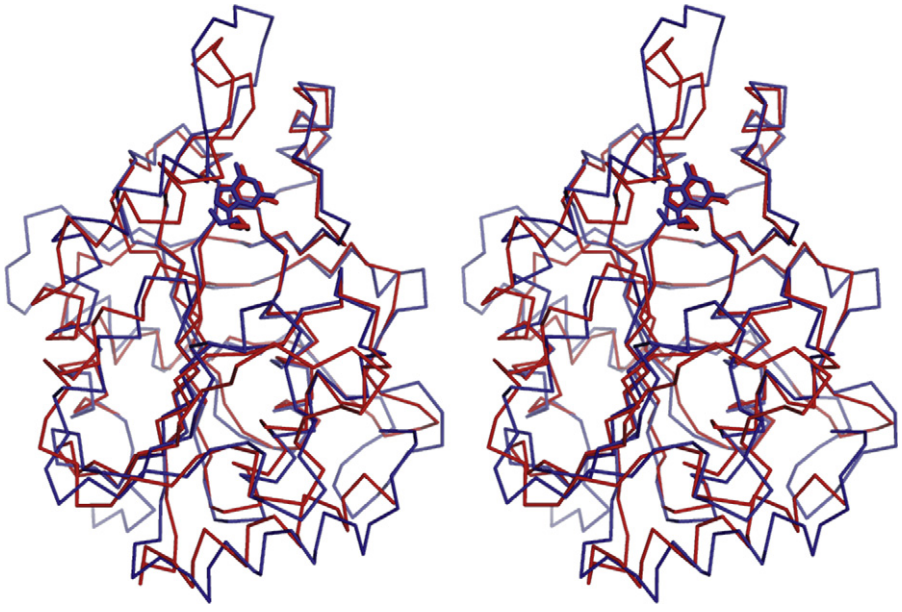

Fig. 5. The Cα superposition of HsPNP:ACY (blue) against MtPNP:ACY:PO_4 (red). The structures are presented as ribbon diagram and the ACY molecule as stick. The structure is shown in stereoview. (For interpretation of the references to colour in this figure legend, the reader is referred to the web version of this article.)

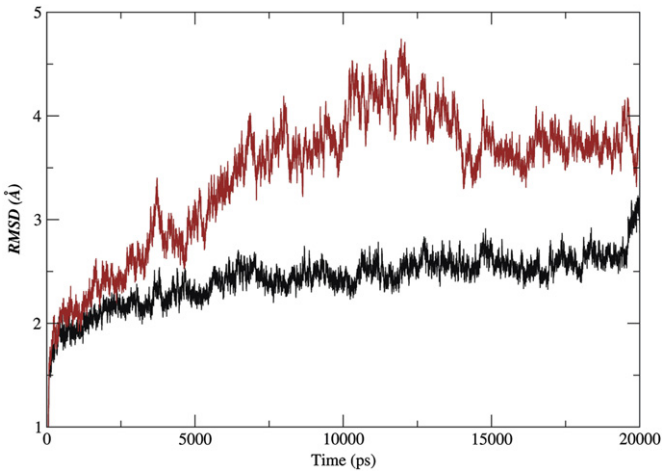

Fig. 6. RMSD of unbound MtPNP (black line) and MtPNP:ACY:PO_4 (red line) systems. (For interpretation of the references to colour in this figure legend, the reader is referred to the web version of this article.)

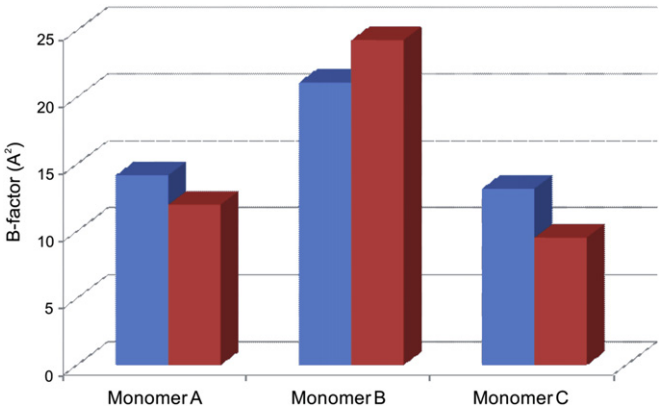

Fig. 8. Calculated B-factor of monomers which compose the unbound MtPNP (blue line) and MtPNP:ACY:PO_4 (red line). (For interpretation of the references to colour in this figure legend, the reader is referred to the web version of this article.)

MtPNP:ACY:PO_4 throughout MD simulations. After rapid increase during the first 100 ps, the protein backbone RMSD average and standard deviation over the 20 ns of the MtPNP system trajectory was 2.4 ± 0.2 Å and the MtPNP:ACY:PO_4 system was 3.4 ± 0.6 Å. It can be seen that the MtPNP simulation has reached an equilibrated state after 500 ps; however, the MtPNP:ACY:PO_4 system reached equilibrium after 15 ns.

The stability and the influence of ACY over the quaternary structure during the MD simulations were assessed by the RG. RG as a function of time is shown in Fig. 7A. The mean values of the RG averaged over the period from 0 to 20 ns of each monomer were determined, giving 27.9 ± 1.2 Å and 28.3 ± 1.6 Å for MtPNP and MtPNP:ACY:PO_4, respectively. Monomers A, B and C present an RG of: 17.9 ± 0.13 Å, 17.8 ± 0.09 Å, and 17.6 ± 0.07 Å, respectively (Fig. 7B).

RG remains essentially constant after 200 ps for both systems, suggesting that the molecular conformation was significantly preserved as a whole. This analysis suggests that RG centered on the center of mass of the trimeric MtPNP remains essentially constant, indicating that the monomers of MtPNP structure remain in the trimeric state, which is the biological unit for MtPNP.

3.6. The role of Phe153 in MtPNP

As demonstrated in previous MD studies [8,46–48], Phe159 from HsPNP presents an important structural behavior, working like a lid mechanism in the binding pocket of the adjacent subunit. In *M. tuberculosis*, nevertheless, Phe153 does not seem to play the same role. Fig. 8 shows that B-factor values are not affected by the presence of ACY in the binding pocket as in HsPNP [8,48], thus suggesting that Phe153 does not maintain any kind of interaction with the active binding site making hydrophobic contact and, therefore, no involvement in $\pi-\pi$ interactions with the base

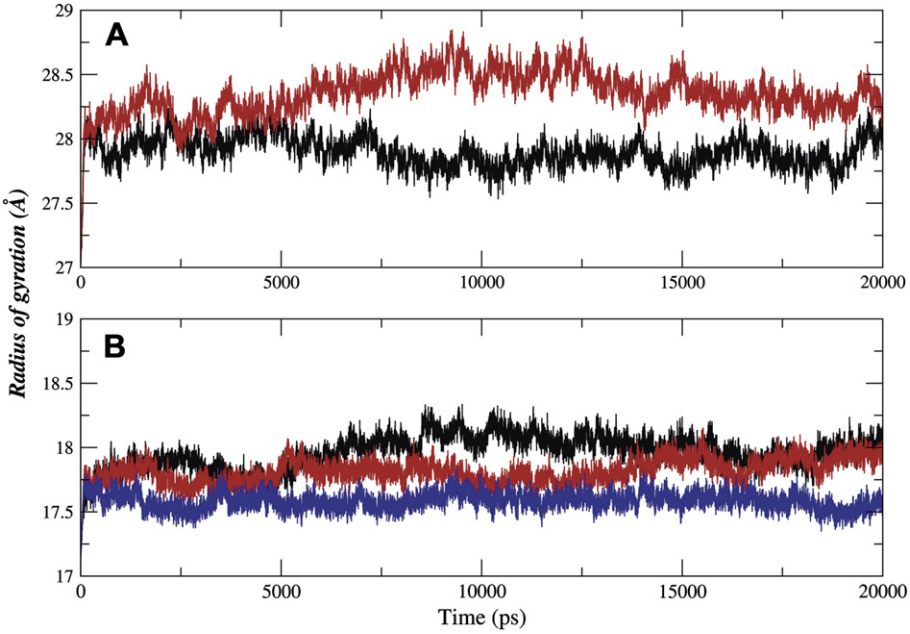

Fig. 7. (A) Radius of gyration between unbound MtPNP (black line) and MtPNP:ACY:PO_4 (red line). (B) Radius of gyration between MtPNP:ACY:PO_4 monomers. Monomer A is bounded to ACY and PO_4 (black line), monomer B is bounded to ACY (red line), and monomer C in free form (blue line). (For interpretation of the references to colour in this figure legend, the reader is referred to the web version of this article.)

Table 3
Eigenvalues (EV) and cumulative eigenvalues (CV) of the covariance matrix resulting from unbound MtPNP and MtPNP:ACY:PO_4 simulations.

Structure	Eigenvector	Monomer A		Monomer B		Monomer C		Structure	Eigenvector	Monomer A		Monomer B		Monomer C	
		EV[a]	CV[b]	EV	CV	EV	CV			EV	CV	EV	CV	EV	CV
MtPNP unbound	1	68.09	24.52	136.66	37.24	47.97	20.96	MtPNP:ACY:PO_4	1	90.10	26.81	120.40	29.09	48.83	40.76
	2	38.16	38.26	24.94	44.03	21.93	30.54		2	39.29	38.21	41.86	39.20	16.69	27.56
	3	12.64	42.81	17.39	48.77	10.34	35.05		3	25.00	45.65	38.21	48.43	13.88	33.39
	4	11.44	46.94	13.65	42.49	9.61	39.25		4	16.68	50.62	16.87	52.51	13.22	38.95
	5	9.54	50.37	11.20	55.54	8.02	42.76		5	13.64	54.67	14.21	55.95	10.38	43.32
	6	7.53	53.08	9.05	58.00	7.22	45.91		6	9.88	57.61	13.42	59.19	6.78	46.17
	7	5.79	55.17	8.16	60.23	6.52	48.76		7	8.17	60.05	11.41	61.94	6.59	48.94
	8	5.42	57.12	7.00	62.13	5.10	50.99		8	6.51	61.98	8.12	63.91	5.59	51.29
	9	4.56	58.76	6.07	63.79	4.46	52.93		9	6.29	63.86	6.99	65.59	4.96	53.38
	10	4.16	60.26	5.85	65.38	3.94	54.65		10	5.20	64.40	6.29	67.11	4.79	55.39

[a] Eigenvalues of covariance matrix (A^2).
[b] Cumulative sum values (%).

moiety, as observed in other trimeric PNPs [5]. This is supported by the data in Tables S1 and S2, where the interactions between the protein and ACY were monitored along MD simulations and testifying the displacement of ACY from the purine base binding site. In fact, the role of Phe153 seems to be involved mainly in sugar binding; more precisely, this residue lies close to position 5′ of the sugar group of the substrate. Nevertheless, the same behavior herein observed was identified in MtPNP associated with Inosine and Hypoxanthine [R.A. Caceres, L.F.S.M Timmers, R.G. Ducati, L.A. Rosado, L.A. Basso, D.S. Santos, W.F. de Azevedo Jr., Combining crystallographic, thermodynamic, and molecular dynamics studies of *M. tuberculosis* purine nucleoside phosphorylase, unpublished results].

3.7. Principal component analysis

Apart from conventional structural and geometrical analysis to assess the stability of the simulations, PCA is utilized to identify large concerted motions in MtPNP:ACY:PO_4. We built the covariance matrixes of the atomic fluctuations in an MD trajectory, in which the overall translation and rotation modes have been removed. Elimination of the overall motion was done at each simulation step, and the total removal of these irrelevant motions was ensured by fitting all the structures to the initial structure. It has been shown that it is sufficient to use only the Cα atomic positions when building the covariance matrix [49]. The matrix is built considering structures sampled every 0.5 ps from the production run of the simulations. A total of 262 residues were included in the analysis, and diagonalization of the covariance matrix resulted in 786 eigenvectors.

Table 3 shows the contribution to the overall motion of the first 10 eigenvectors of one singled-out simulation for each structure and the contribution from each monomer in the protein. It can be seen that the first 10 eigenvectors describe a representative percentage of the motions, 60.10% and 62.30% in average, for the trimeric MtPNP and MtPNP:ACY:PO_4, respectively.

The analysis by monomer of the unbound MtPNP simulation has shown that the total positional fluctuations described by the

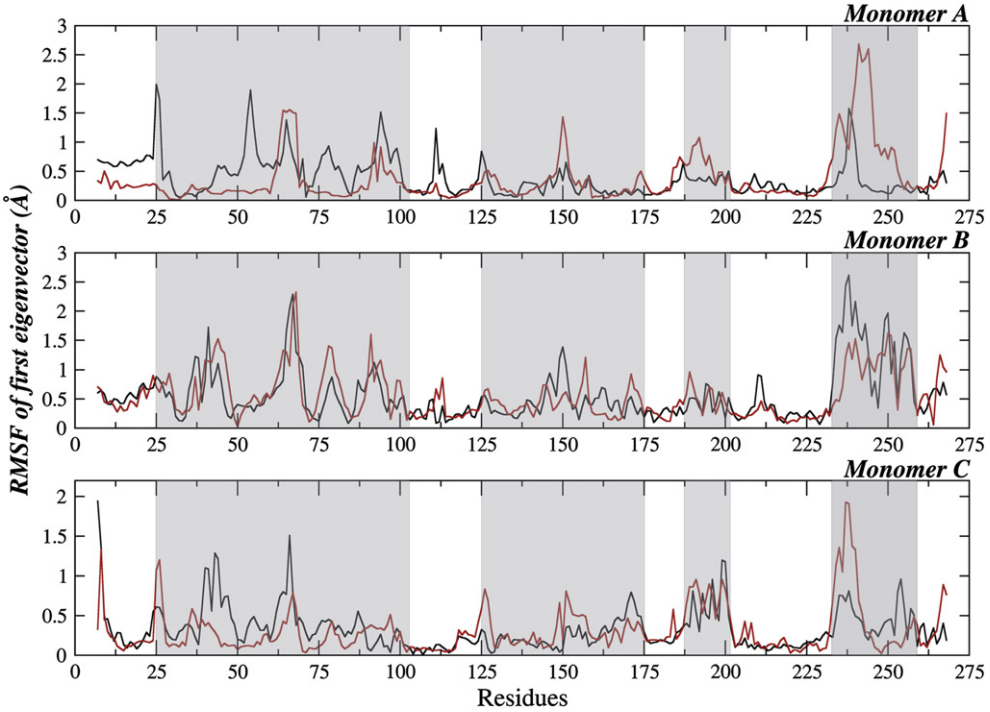

Fig. 9. Displacement of the components of the first eigenvectors for trimeric structures of unbound MtPNP (black line) and MtPNP:ACY:PO_4 (red line). (For interpretation of the references to colour in this figure legend, the reader is referred to the web version of this article.)

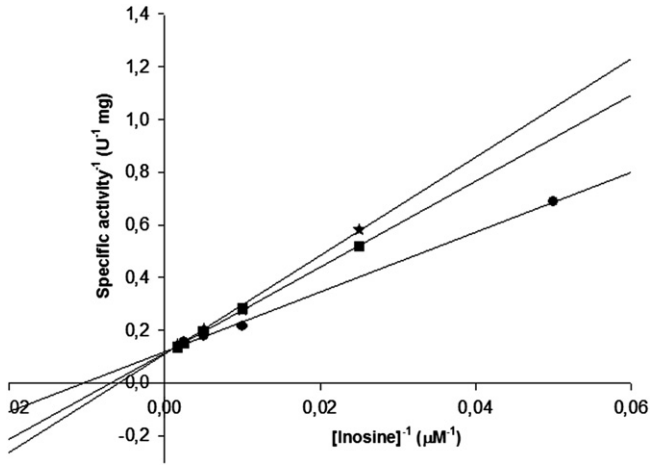

Fig. 10. The double-reciprocal plot reveals an ACY competitive inhibition pattern for MtPNP with respect to Inosine, as the family of lines intersect on the *y* axis. Each curve represents varied-fixed levels of ACY as follows: (●) 0, (■) 32, and (★) 48 nM.

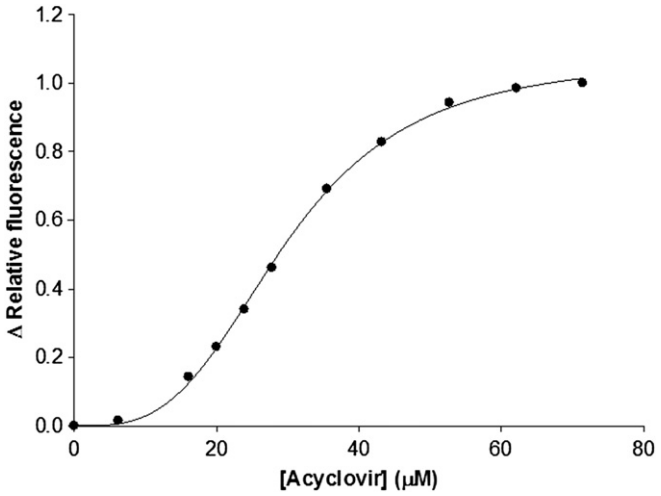

Fig. 12. Overall dissociation constant for MtPNP:ACY binary complex formation monitoring changes in intrinsic protein fluorescence.

first 10 eigenvectors are 60.26%, 65.38%, and 54.65% for monomers A, B, and C, respectively. The results of the first eigenvectors alone represent 24.52% (monomer A), 37.24% (monomer B), and 20.96% (monomer C) of the total motion of the protein. For the MtPNP:ACY:PO_4 complex simulation, the analysis has shown that the total positional fluctuations described by the first 10 eigenvectors are 64.40%, 67.11%, and 55.39% for monomers A, B, and C, respectively. The results of the first eigenvectors alone represent 26.81% (monomer A), 29.09% (monomer B), and 40.76% (monomer C) of the total motion of the protein (Table 3). The significant fluctuations of the first eigenvector are shown in Fig. 9. The main fluctuations are presented for the regions formed by loops, composed by Thr23-Val30, Gly35-Thr49, Ala55-Ala69, Arg88-His102, Asp172-Leu175, Pro191-Leu200 (α-helix), and Asn231-Ser253. However, when complexed with ACY, the regions composed by Thr143-Ser161 and Pro184-Thr190 are localized in the subunit interfaces, and seem to be affected by a decreasing of fluctuation, as would be expected. An interesting finding in the first eigenvector structure is the flexibility of loops Pro184-Thr190 and Asn231-Ser243, which are involved in binding and releasing events in the purine binding site.

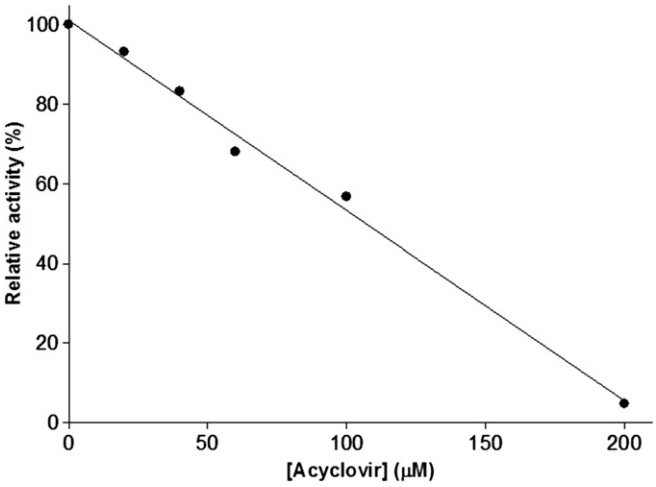

Fig. 11. MtPNP relative activity as a function of ACY concentration.

3.8. Assessment of ACY upon MtPNP activity

Data from ACY inhibition studies were fitted to a Lineweaver–Burk double-reciprocal plot (Fig. 10), and the results demonstrate that ACY is a competitive inhibitor of MtPNP with respect to Inosine, yielding a K_i value of 150 ± 46 nM. A value of 41 ± 3 μM was determined for ACY IC_{50} at near K_M values for the substrates for MtPNP using linear regression (Fig. 11).

3.9. Equilibrium binding of ACY to MtPNP

The enhancement in intrinsic protein fluorescence upon ACY binding to MtPNP was sigmoidal (Fig. 12) and fitting the data to the Hill equation yielded values of 68 ± 8 mM for K' and 3.3 ± 0.1 for n. This result shows that ACY binds to free MtPNP and it is in good agreement with the low degree of cooperativity of ACY binding.

4. Conclusions

The resolution of the MtPNP structure in complex with ACY and PO_4 provided additional information for the structure-based drug design initiatives, since there are very few MtPNP structures solved so far. In addition, as one dissects the MD results, it could be observed that Phe153 from MtPNP does not exhibit the same conformational behavior if compared to Phe159 from HsPNP. The Similarity Ensemble Approach (SEA) [50] demonstrated to be very useful tool. It was used aiming to verify the potential inhibition of ACY. The SEA provided an e-value of 1.12×10^{-122} and a maximum Tanimoto coefficient of 56%, giving indications that ACY could be an inhibitor. Probably, the result provided by the server was due to the purine moiety similarity between ACY and Immucillin, a known potential and established PNP inhibitor. Therewithal, this considerable inhibition may provide some clues, as ACY could be helpful to the development of a potential inhibitor; structure-based drug design initiatives should be carried out aiming at structural modifications and, consequently, increasing the inhibition. In addition, the inhibition data provided by ACY in complex with MtPNP is essential, since such information about inhibitors are sparse and pivotal in the development of specific empirical scoring functions and QSAR models.

4.1. Deposit

The atomic coordinates and structure factors for the MtPNP:ACY:PO_4 structure have been deposited at the Protein Data Bank, access code:3IX2.

Acknowledgments

This work was supported by Millennium Initiative Program and National Institute of Science and Technology in Tuberculosis (INCT-TB), MCT-CNPq, Ministry of Health - Department of Science and Technology (DECIT) - Secretary of Health Policy (Brazil) to L.A.B., D.S.S., and W.F.A. Jr. L.A.B. (CNPq, 520182/99-5), D.S.S. (CNPq, 304051/1975-06), and W.F.A. Jr. are Research Career Awardees of the National Research Council of Brazil (CNPq). R.A.C. would like to thank CNPq for the fellowship, and L.F.S.M.T. would like to thank CAPES for the fellowship. R.G.D is a postdoctoral fellow of CNPq.

Appendix. Supplementary material

Supplementary material associated with this article can be found, in the online version, at doi:10.1016/j.biochi.2011.10.003.

References

[1] WHO, Global Tuberculosis Control: A Short Update to the 2009 Report. World Health, Geneva, Switzerland, December/2009. http://www.who.int/tb/publications/global_report/2009/en/index.html.
[2] P. Nunn, B. Williams, K. Floyd, C. Dye, G. Elzinga, M. Raviglione, Tuberculosis control in the era of HIV, Nat. Rev. Immunol. 5 (2005) 819–826.
[3] R.G. Ducati, A. Ruffino-Netto, L.A. Basso, D.S. Santos, The resumption of consumption – a review on tuberculosis, Mem. Inst. Oswaldo Cruz 101 (2006) 697–714.
[4] S.T. Cole, R. Brosch, J. Parkhill, T. Garnier, C. Churcher, D. Harris, S.V. Gordon, K. Eiglmeier, S. Gas, C.E. Barry, F. Tekaia, K. Badcock, D. Basham, D. Brown, T. Chillingworth, R. Connor, R. Davies, K. Devlin, T. Feltwell, S. Gentles, N. Hamlin, S. Holroyd, T. Hornsby, K. Jagels, A. Krogh, J. McLean, S. Moule, L. Murphy, K. Oliver, J. Osborne, M.A. Quail, M.A. Rajandream, J. Rogers, S. Rutter, K. Seeger, J. Skelton, R. Squares, S. Squares, J.E. Sulston, K. Taylor, S. Whitehead, B.G. Barrell, Deciphering the biology of *Mycobacterium tuberculosis* from the complete genome sequence, Nature 393 (1998) 537–544.
[5] R.G. Ducati, A.A. Souto, R.A. Caceres, W.F. de Azevedo Jr., L.A. Basso, D.S. Santos, Purine nucleoside phosphorylase as a molecular target to develop active compounds against *Mycobacterium tuberculosis*, Int. Rev. Biophys. Chem. 1 (2010) 34–40.
[6] H.M. Kalckar, Differential spectrophotometry of purine compounds by means of specific enzymes determination of hydroxypurine compounds, J. Biol. Chem. 167 (1947) 429–443.
[7] R.G. Ducati, A. Breda, L.A. Basso, D.S. Santos, Purine salvage pathway in *Mycobacterium tuberculosis*, Curr. Med. Chem. 18 (2011) 1258–1275.
[8] L.F. Timmers, R.A. Caceres, A.L. Vivan, L.M. Gava, R. Dias, R.G. Ducati, L.A. Basso, D.S. Santos, W.F. de Azevedo Jr., Structural studies of human purine nucleoside phosphorylase. Towards a new specific empirical scoring function, Arch. Biochem. Biophys. 479 (2008) 28–38.
[9] M.J. Pugmire, S.E. Ealick, Structural analyses reveal two distinct families of nucleoside phosphorylases, Biochem. J. 361 (2002) 1–25.
[10] W.F. de Azevedo Jr., F. Canduri, D.M. dos Santos, R.G. Silva, J.S. de Oliveira, L.P. de Carvalho, L.A. Basso, M.A. Mendes, M.S. Palma, D.S. Santos, Crystal structure of human purine nucleoside phosphorylase at 2.3 Å resolution, Biochem. Biophys. Res. Commun. 308 (2003) 545–552.
[11] F. Canduri, V. Fadel, L.A. Basso, M.S. Palma, D.S. Santos, W.F. de Azevedo Jr., New catalytic mechanism for human purine nucleoside phosphorylase, Biochem. Biophys. Res. Commun. 327 (2005) 646–649.
[12] C. Mao, W.J. Cook, M. Zhou, G.W. Koszalka, T.A. Krenitsky, S.E. Ealick, The crystal structure of *Escherichia coli* purine nucleoside phosphorylase: a comparison with the human enzyme reveals a conserved topology, Structure 5 (1997) 1373–1383.
[13] L.A. Basso, D.S. Santos, W. Shi, R.H. Furneaux, P.C. Tyler, V.L. Schramm, J.S. Blanchard, Purine nucleoside phosphorylase from *Mycobacterium tuberculosis*. Inhibition by a transition-state analogue and dissection by parts, Biochemistry 40 (2001) 8196–8203.
[14] R.G. Ducati, D.S. Santos, L.A. Basso, Substrate specificity and kinetic mechanism of purine nucleoside phosphorylase from *Mycobacterium tuberculosis*, Arch. Biochem. Biophys. 486 (2009) 155–164.
[15] A. Bzowska, E. Kulikowska, D. Shugar, Properties of purine nucleoside phosphorylase (PNP) of mammalian and bacterial origin, Z. Naturforsch. C. 45 (1990) 59–70.
[16] K.F. Jensen, Purine-nucleoside phosphorylase from *Salmonella typhimurium* and *Escherichia coli*. Initial velocity kinetics, ligand banding, and reaction mechanism, Eur. J. Biochem. 61 (1976) 377–386.
[17] J. Tebbe, A. Bzowska, B. Wielgus-Kutrowska, W. Schröder, Z. Kazimierczuk, D. Shugar, W. Saenger, G. Koellner, Crystal structure of the purine nucleoside phosphorylase (PNP) from *Cellulomonas sp.* and its implication for the mechanism of trimeric PNPs, J. Mol. Biol. 294 (1999) 1239–1255.
[18] T.H. Tahirov, E. Inagaki, N. Ohshima, T. Kitao, C. Kuroishi, Y. Ukita, K. Takio, M. Kobayashi, S. Kuramitsu, S. Yokoyama, M. Miyano, Crystal structure of purine nucleoside phosphorylase from *Thermus thermophilus*, J. Mol. Biol. 337 (2004) 1149–1160.
[19] W. Shi, L.A. Basso, D.S. Santos, P.C. Tyler, R.H. Furneaux, J.S. Blanchard, S.C. Almo, V.L. Schramm, Structures of purine nucleoside phosphorylase from *Mycobacterium tuberculosis* in complexes with immucillin-H and its pieces, Biochemistry 40 (2001) 8204–8215.
[20] R.G. Ducati, L.A. Basso, D.S. Santos, W.F. de Azevedo Jr., Crystallographic and docking studies of purine nucleoside phosphorylase from *Mycobacterium tuberculosis*, Bioorg. Med. Chem. 18 (2010) 4769–4774.
[21] W.B. Parker, M.C. Long, Purine metabolism in *Mycobacterium tuberculosis* as a target for drug development, Curr. Phar. Des. 13 (2007) 599–608.
[22] J.V. Tuttle, T.A. Krenitsky, Effects of acyclovir and its metabolites on purine nucleoside phosphorylase, J. Biol. Chem. 259 (1984) 4065–4069.
[23] Collaborative Computational Project Number 4, The CCP4 suite: programs for protein, Acta Crystallogr. D Biol. Crystallogr. 50 (1994) 760–763.
[24] J. Navaza, Implementation of molecular replacement in AMoRe, Acta Crystallogr. D Biol. Crystallogr. 57 (2001) 1367–1372.
[25] R.A. Laskowski, M.W. MacArthur, D.S. Moss, J.M. Thornton, PROCHECK: a program to check the stereochemical quality of protein structures, J. Appl. Cryst. 26 (1993) 283–291.
[26] B. Hess, C. Kutzner, D. van der Spoel, E. Lindahl, GROMACS 4: algorithms for highly efficient, load-Balanced, and scalable molecular simulation, J. Chem. Theory Comput. 4 (2008) 435–447.
[27] D. van der Spoel, E. Lindahl, B. Hess, G. Groenhof, A.E. Mark, H.J. Berendsen, GROMACS: fast, flexible, and free, J. Comp. Chem. 26 (2005) 1701–1718.
[28] C. Ooestenbrink, T.A. Soares, N.F. van der Vegt, W.F. van Gunsteren, Validation of the 53A6 GROMOS force field, Eur. Biophys. J. 34 (2005) 273–284.
[29] D.M. van Aalten, B. Bywater, B. Findlay, M. Hendlich, R.W. Hooft, G. Vriend, PRODRG, a program for generating molecular topologies and unique molecular descriptors from coordinates of small molecules, Comput. Aided Mol. Des. 10 (1996) 255–262.
[30] C.M. Breneman, K.B. Wiberg, Determining atom-centered monopoles from molecular electrostatic potentials, the need for high sampling density in formamide conformational analysis, J. Comput. Chem. 11 (1990) 361–373.
[31] M.J. Frisch, G.W. Trucks, H.B. Schlegel, G.E. Scuseria, M.A. Robb, J.R. Cheeseman, J.A. Montgomery Jr., T. Vreven, K.N. Kudin, J.C. Burant, J.M. Millam, S.S. Iyengar, J. Tomasi, V. Barone, B. Mennucci, M. Cossi, G. Scalmani, N. Rega, G.A. Petersson, H. Nakatsuji, M. Hada, M. Ehara, K. Toyota, R. Fukuda, J. Hasegawa, M. Ishida, T. Nakajima, Y. Honda, O. Kitao, H. Nakai, M. Klene, X. Li, J.E. Knox, H.P. Hratchian, J.B. Cross, C. Adamo, J. Jaramillo, R. Gomperts, R.E. Stratmann, O. Yazyev, A.J. Austin, R. Cammi, C. Pomelli, J.W. Ochterski, P.Y. Ayala, K. Morokuma, G.A. Voth, P. Salvador, J.J. Dannenberg, V.G. Zakrzewski, S. Dapprich, A.D. Daniels, M.C. Strain, O. Farkas, D.K. Malick, A.D. Rabuck, K. Raghavachari, J.B. Foresman, J.V. Ortiz, Q. Cui, A.G. Baboul, S. Clifford, J. Cioslowski, B.B. Stefanov, G. Liu, A. Liashenko, P. Piskorz, I. Komaromi, R.L. Martin, D.J. Fox, T. Keith, M.A. Al-Laham, C.Y. Peng, A. Nanayakkara, M. Challacombe, P.M.W. Gill, B. Johnson, W. Chen, M.W. Wong, C. Gonzalez, J.A. Pople, Gaussian 03, Revision B.05. Gaussian, Inc., Pittsburgh, PA, 2003.
[32] H.J.C. Berendsen, J.R. Grigera, T.P. Straatsma, The missing term in effective pair potentials, J. Phys. Chem. 91 (1987) 6269–6271.
[33] G. Bussi, D. Donadio, M. Parrinello, Canonical sampling through velocity rescaling, J. Chem. Phys. 126 (2007) 014101-1–014101-7.
[34] H.J.C. Berendsen, J.P.M. Postma, W.F. van Gunsteren, A. DiNola, J.R. Haak, Molecular dynamics with coupling to an external bath, J. Chem. Phys. 81 (1984) 3684–3690.
[35] B. Hess, H. Bekker, H.J.C. Berendsen, J.G.E.M. Fraaije, LINCS: a linear constraint solver for molecular simulations, J. Comput. Chem. 18 (1997) 1463–1472.
[36] T. Darden, D. York, L. Pedersen, Particle mesh Ewald: an N log(N) method for Ewald sums in large systems, J. Chem. Phys. 98 (1993) 10089–10092.
[37] N. Guex, M.C. Peitsch, SWISS-MODEL and the Swiss-PdbViewer: an environment comparative protein modeling, Electrophoresis 18 (1997) 2714–2723.
[38] W. Humphrey, A. Dalke, K. Schulten, VMD: visual molecular dynamics, J. Mol. Graph. 14 (1996) 33–38.
[39] W.L. Delano, J.W. Lam, PyMOL: a communications tool for computational models, Abstr. Pap. Am. Chem. Soc. 230 (2005) U1371–U1372.
[40] N.M. Mascarenhas, D. Bhattacharyya, N. Ghoshal, Why pyridine containing pyrido[2,3-d]pyrimidin-7-ones selectively inhibit CDK4 than CDK2: insights from molecular dynamics simulation, J. Mol. Graph. Model. 28 (2010) 695–706.
[41] A. Amadei, A.B. Linssen, H.J. Berendsen, Essential dynamics of proteins, Proteins 17 (1993) 412–425.
[42] D.E. McRee, Differential evolution for protein crystallographic optimizations, Acta Crystallogr. D Biol. Crystallogr. 60 (2004) 2276–2279.
[43] D.O. Nolasco, F. Canduri, J.H. Pereira, J.R. Cortinóz, M.S. Palma, J.S. Oliveira, L.A. Basso, W.F. de Azevedo Jr., D.S. Santos, Crystallographic structure of PNP

from *Mycobacterium tuberculosis* at 1.9Å resolution, Biochem. Biophys. Res. Commun. 324 (2004) 789–794.
[44] A.C. Wallace, R.A. Laskowski, J.M. Thornton, LIGPLOT: a program to generate schematic diagrams of protein-ligand interactions, Protein Eng. 8 (1995) 127–134.
[45] D.M. dos Santos, F. Canduri, J.H. Pereira, M.V.B. Dias, R.G. Silva, M.A. Mendes, M.S. Palma, L.A. Basso, W.F. de Azevedo Jr., D.S. Santos, Crystal structure of purine nucleoside phosphorylase complexed with acyclovir, Biochem. Biophys. Res. Commun. 308 (2003) 553–559.
[46] L.F. Timmers, R.A. Caceres, R. Dias, L.A. Basso, D.S. Santos, W.F. de Azevedo Jr., Molecular modeling, dynamics and docking studies of purine nucleoside phosphorylase from *Streptococcus pyogenes*, Biophys. Chem. 142 (2009) 7–16.
[47] R.A. Caceres, L.F.S. Timmers, R. Dias, L.A. Basso, D.S. Santos, W.F. de Azevedo Jr., Molecular modeling and dynamics simulations of PNP from *Streptococcus agalactiae*, Bioorgan. Med. Chem. 16 (2008) 4984–4993.
[48] R.A. Caceres, L.F. Timmers, I. Pauli, L.M. Gava, R.G. Ducati, L.A. Basso, D.S. Santos, W.F. de Azevedo Jr., Crystal structure and molecular dynamics studies of human purine nucleoside phosphorylase complexed with 7-deazaguanine, J. Struct. Biol. 169 (2010) 379–388.
[49] B. Hess, Similarities between principal components of protein dynamics and random diffusion, Phys. Rev. E. Stat. Phys. Plasmas Fluids Relat. Interdiscip. Top. 62 (2000) 8438–8448.
[50] M.J. Keiser, B.L. Roth, B.N. Armbruster, P. Ernsberger, J.J. Irwin, B.K. Shoichet, Relating protein pharmacology by ligand chemistry, Nat. Biotechnol. 25 (2007) 197–206.